J. Fluid Mech. (1992), *vol.* 241, *pp.* 705–722
Printed in Great Britain

An advanced experimental investigation of quasi-two-dimensional shear flows

By F. V. DOLZHANSKII, V. A. KRYMOV AND D. YU. MANIN
Institute of Atmospheric Physics, Russian Academy of Sciences,
Pyzhevsky 3, 109017 Moscow, Russia

(Received 28 June 1991 and in revised form 5 February 1992)

Forced shear flows in a thin layer of an incompressible viscous fluid are studied experimentally. Streak photographs are used to obtain the stream function of vortical flow patterns arising after the primary shear flow loses stability. Various flow characteristics are determined and results are compared to the stability theory of quasi-two-dimensional flows. The applicability of the quasi-two-dimensional approximation is directly verified and the possibility of reconstruction of the driving force from the secondary flow pattern is demonstrated.

1. Introduction. What is a quasi-two-dimensional flow?

Strictly two-dimensional (2D) flows, as solutions of hydrodynamic equations, constitute a class of great importance and variety. In particular, a well-developed theory is that of the 2D stability of shear flows. Though it has a number of possible applications in nature, technology and laboratory experiment, one cannot directly apply strictly 2D theory to real flows. The reason is that real 2D flows are either subject to 3D instability, or their two-dimensionality is maintained by external factors that also affect stability. Most commonly these are solid boundaries (bottom and/or top), perhaps together with general rotation, transverse magnetic field, etc. This leads to the breakdown of strict two-dimensionality, in that velocity components now depend strongly on the transverse coordinate due to boundary layers arising on the bottom and top. However if the transverse ('vertical') velocity is small compared to the horizontal velocity, this vertical dependence can be parametrized via an 'external friction' term, $-\lambda \boldsymbol{v}$, in the right-hand side of the 2D equation of motion ($\boldsymbol{v}$ is the horizontal velocity, and λ the decrement of the external friction):

$$\partial_t \boldsymbol{v} + (\boldsymbol{v}\cdot\boldsymbol{\nabla})\,\boldsymbol{v} = -\boldsymbol{\nabla} p - \lambda \boldsymbol{v} + \boldsymbol{f} \tag{1}$$

(p denotes the ratio of pressure to density). We shall identify flows governed by this equation as *quasi-two-dimensional* (Q2D). This equation can be derived for various hydrodynamical systems via expansion in some small parameter. Consequently the expression for λ depends on the underlying physics. For instance, $\lambda \approx 2\nu/h^2$ (Rayleigh friction) for a thin non-rotating fluid layer of thickness h and viscosity ν, $\lambda = (\Omega\nu)^{\frac{1}{2}}/h$ (Ekman friction) for a layer rotating at angular velocity Ω about a vertical axis, and it is given by a similar formula for electrically conducting layer in a vertical magnetic field (Hartmann friction). In fact, all three cases can be unified by writing

$$\lambda = \nu/h_*^2,$$

where $h_*^2 = \frac{1}{2}h^2$ for a thin layer and $h_*^2 = h\delta$, δ being the Ekman or Hartmann layer

thickness: $\delta = \delta_E = (\nu/\Omega)^{\frac{1}{2}}$ or $\delta = \delta_H = cB^{-1}(\rho\nu/\sigma)^{\frac{1}{2}}$ (c is the speed of light, B is the magnetic induction, ρ is the fluid density and σ its conductivity); see Dolzhanskii, Krymov & Manin (1990) and Dolzhanskii & Manin (1990).

A fundamental distinction from the strictly 2D situation is that Q2D flows are controlled by two dimensionless parameters, namely the traditional Reynolds number $\mathbb{R}_\nu = UD/\nu$ and the Reynolds number in terms of the external friction $\mathbb{R}_\lambda = U/\lambda D$ (where U and D are the characteristic length and velocity scales of the flow). Dolzhanskii (1987) has shown that in the case $\mathbb{R}_\lambda \ll \mathbb{R}_\nu$ there is no dependence on $\mathbb{R}_\nu$, and the internal viscosity term ($\nu\nabla^2 v$) can be neglected, at least in stability considerations. Moreover, the condition of quasi-two-dimensionality itself is equivalent to the above inequality, $\mathbb{R}_\lambda \ll \mathbb{R}_\nu$, which is the reason why this term is not included in (1). Experimental results on the stability of Kolmogorov shear flow were explained through incorporation of the external friction in Gledzer, Dolzhanskii & Oboukhov (1981). Equation (1) was used to describe experimental results by Niino (1982) and Niino & Misawa (1984) (Ekman friction, see also Busse 1968), and by Rabaud & Couder (1983) and Chomaz *et al.* (1988) (Rayleigh friction). Both cases are in a sense degenerate, since $\mathbb{R}_\lambda$ is equal to $\mathbb{R}_\nu$ in experiments where the flow is driven by differentially rotating parts of the bottom of a tank filled by fluid. Dolzhanskii (1987) has also demonstrated the structural instability of strictly 2D theory when small external friction is involved. Other results concerning nonlinear stability and experimental simulations obtained to date can be found in the reviews by Dolzhanskii *et al.* (1990) and Dolzhanskii, Krymov & Manin (1991).

This work has several closely connected but distinct goals. First, we present a method for experimental flow field assimilation which yields a 2D stream function stored in a computer memory. With such a data set at hand one can obtain all relevant information provided that not too much numerical differentiation is required. Second, we demonstrate that the assimilation algorithm is able to fill 'blank spots' devoid of original data. Next, we use the real data obtained in the experiment to calculate the external friction coefficient λ and the profile of the force which maintains the flow (this is also a problem of practical importance in dynamic meteorology). This is done on the assumption that the flow is governed by the Q2D equation (1). So when consistent results are obtained this is also a check of the validity of the Q2D approximation itself.

2. Experimental set-up

The experimental flow was generated in the MHD-type apparatus described previously in Dovzhenko, Novikov & Oboukhov (1979). A set of circular magnets (figure 1*a*) created an axially symmetric magnetic field with its vertical component changing sign at certain radii (5.8, 10.4 and 15.2 cm). A circular pan with a relatively thin fluid layer was placed on top of the magnets. A solution of $CuSO_4$ in water ($\rho = 1.07$ g/cm^3, $\nu = 0.012$ cm^2/s) was used. A direct electric current could run between two circular electrodes mounted concentrically in the pan, resulting in an Ampère force acting on the fluid in the azimuthal direction. The radial profile of the force depended on the magnetic field profile (which could be controlled to some extent by changing the clearance between magnets and the pan), and on the position and shape of electrodes. The velocity profile generated by the force applied also depends on the depth of the fluid layer.

To produce a simple shear we used cylindrical electrodes placed inside and outside the 'zero line' ($R_0 = 10.4$ cm) of the magnetic field. The sine-type velocity profile was

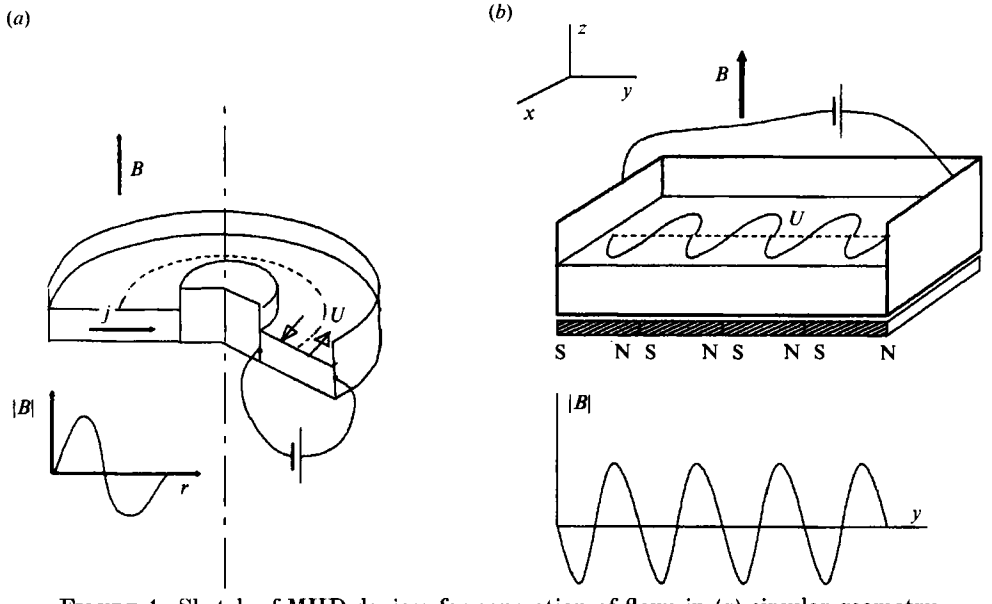

FIGURE 1. Sketch of MHD devices for generation of flows in (*a*) circular geometry and (*b*) Kolmogorov flow.

created at layer depth $h = 10$ mm and electrode radii $r_i = 5.8$ cm and $r_o = 15.0$ cm. The tanh-type profile was studied in the channel with $r_i = 6.0$ cm and $r_o = 14.8$ cm in the range 3 mm $\leqslant h \leqslant 5$ mm. In addition to cylindrical electrodes, we used rings placed flat on the bottom of the pan, at $r_i = 7.5$ cm and $r_o = 8.5$ cm, to obtain unidirectional jet flow not confined by lateral boundaries (the fluid could move above the ring electrodes). The thickness of the Hartmann boundary layer δ_H always exceeded 1 m, so that the fluid motion had no effect on the magnetic field (recall that $\delta_H \gg h$ is the condition for no $\boldsymbol{B} \leftarrow \boldsymbol{v}$ feedback).

A similar device was used to generate Kolmogorov flow in a rectangular domain. A cuvette of dimensions 27×17.6 cm with fluid layer of depth 4 mm was placed on a set of four magnetic rubber bands, each 27 cm long, so that the magnetic field was periodic in the transverse direction with four periods (4×4.4 cm). Electric current ran between two electrodes placed at the lateral boundaries of the cuvette (figure 1*b*).

Flow was visualized with aluminium powder floating on the surface of the fluid. Pictures of the flow were taken from above and streak photographs were processed as described in §4.

3. Principal features of experimental flows

We provide here a brief description of previous experimental results obtained by Dovzhenko & Krymov (1983), Krymov (1989) and Krymov & Manin (1989) as background for the new results. (See also the review by Dolzhanskii *et al.* 1990, where experimental results by different authors were interpreted in terms of the Q2D stability theory.) Characteristic flow velocities obtained in the experiment ranged from 1 mm/s to several cm/s. With small forcing the flow was laminar and axially symmetric. Since all flows under study were of shear type (had an inflexion point) they lose stability at a specific magnitude of forcing. According to the Q2D theory, the onset of instability is determined by $\mathbb{R}_\lambda$, the critical valuc being approximately

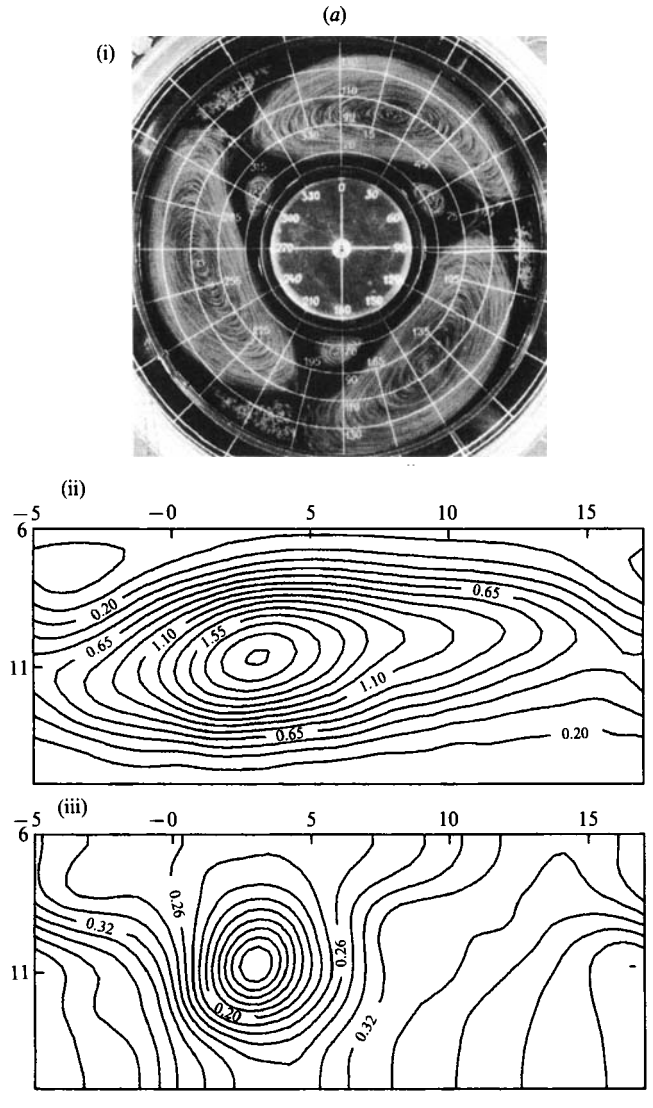

FIGURE 2(*a*). For caption see page 711.

independent of the velocity profile and of the order $\mathbb{R}_\lambda^* \approx 6$–8. In fact, the stability criterion is given by

inviscid increment of 2D instability = decrement due to the external friction.

Here the left-hand side is determined from the Rayleigh equation and depends weakly on the flow velocity profile, while the right-hand side is the λ coefficient, non-dimensionalized by a characteristic flow length and velocity, which gives $\lambda D/U = \mathbb{R}_\lambda^{-1}$.

Loss of stability leads to a circular train of vortices taking the place of the axially symmetric flow (see figure 2). (For the Kolmogorov flow a 'parquet floor' vortex pattern develops.) At first the vortices are weak and of equal size, and the dimensionless wave number $\alpha_0 = n_0 D/R_0$ is of the order 0.4–0.5, in accordance with the linear theory (n_0 is the total number of vortices). With increasing forcing, the

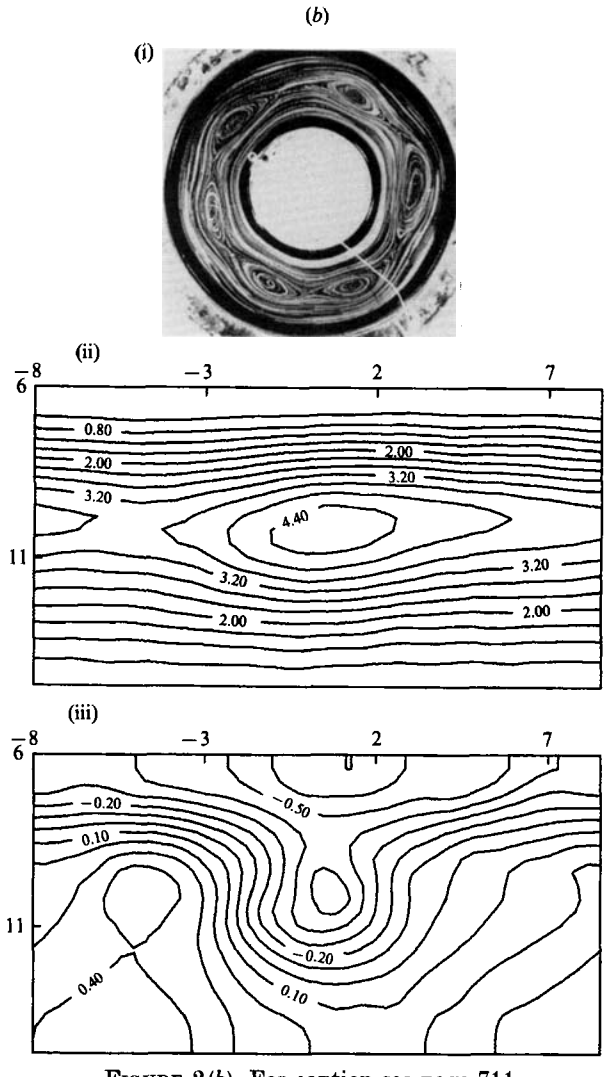

FIGURE 2(*b*). For caption see page 711.

vortices first grow in intensity and then in size, while their number decreases. Oscillations can also start, as well as hysteresis and non-uniqueness phenomena. This is, however, beyond the scope of the present work. Here we deal with relatively small supercriticalities, $s = \mathbb{R}_\lambda/\mathbb{R}_\lambda^* - 1 \lesssim 3$, when the flow is stationary and unique at a given $\mathbb{R}_\lambda$. It should be noted that in processing experimental data we used $s = I/I^* - 1$, where I is the net electric current through the fluid layer, and I^* its critical value. In our experimental configuration I is proportional to the Reynolds number based on the Ampère force.

4. Processing of streak photographs

In order to improve and facilitate interpretation of experimental results we used a computer technique similar (though not identical) to that described in Sommeria, Meyers & Swinney (1988). It consisted of the following steps.

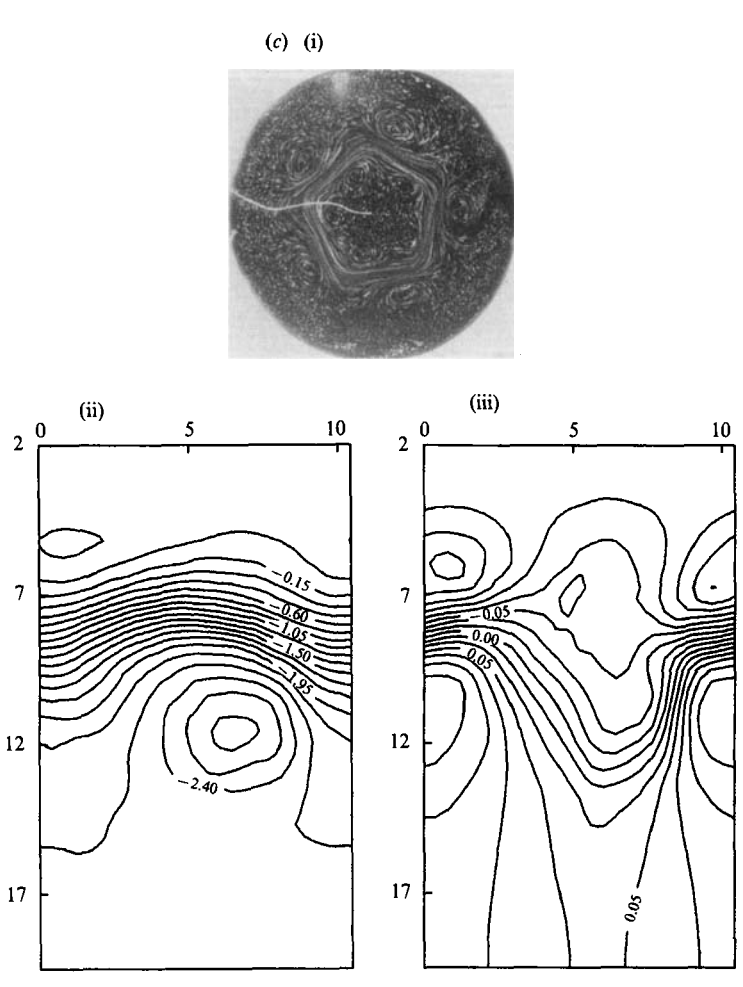

FIGURE 2(c). For caption see facing page.

(i) The beginning and end of each streak in a photograph of the flow was recorded in a disk file with the aid of a digitizing tablet.

(ii) The whole experimental domain (i.e. the ring $r_i < r < r_o$) was divided into n_0 (the number of vortices) sectors, $2\pi k/n_0 < \phi < 2\pi(k+1)/n_0$, $k \in [0, n_0 - 1]$, each sector containing one vortex, and streaks corresponding to the kth vortex were rotated through the angle $-2\pi k/n_0$, so that all vortices were superimposed.

(iii) Each streak was treated as a velocity vector; a velocity field $v(r, \phi)$ was obtained by interpolation on a regular grid with two-dimensional cubic splines. For circular flows the grid was rectangular in the $(r, R_0\phi)$-plane and cylindrical coordinates (r, ϕ) were used in subsequent calculations.

(iv) The vorticity field $\zeta(r, \phi)$ was obtained by numerical differentiation of the velocity, $\zeta = \nabla_z \times v$.

(v) The stream function $\Psi(r, \phi)$ was determined by numerically solving the Poisson equation

$$\nabla^2 \Psi = -\zeta \tag{2}$$

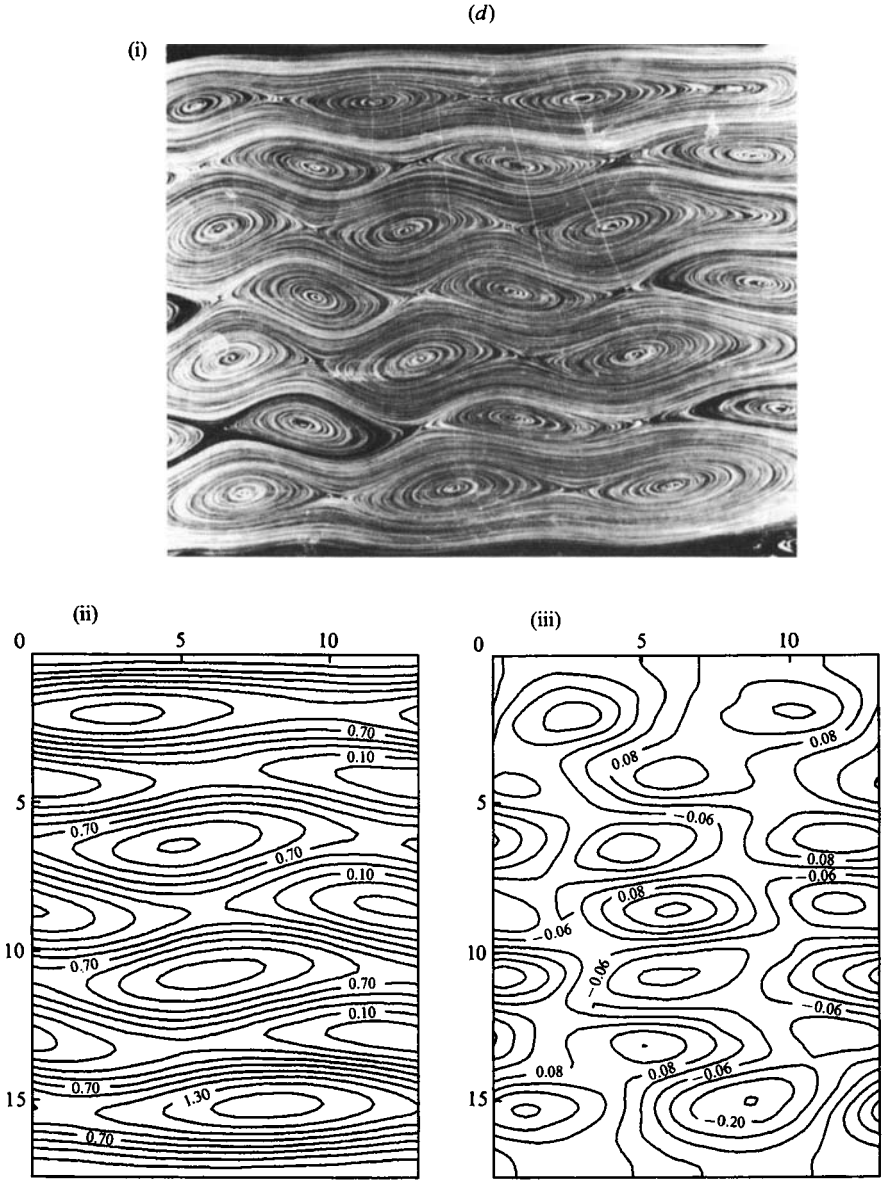

FIGURE 2. (i) Flow pattern, (ii) stream function topography (cm^2/s), and (iii) pressure topography (cm^2/s^2), for flow with (*a*) sine-type velocity profile at $s = 1.0$, (*b*) tanh-type velocity profile at $s = 0.86$, (*c*) jet flow at $s = 1.85$, and (*d*) Kolmogorov flow at $s = 0.53$.

with boundary conditions $\Psi = 0$ at $r = r_i$ and $\Psi = J_0$ at $r = r_o$, where J_0 is the total flux,

$$J_0 = \int_{r_i}^{r_o} v_\phi \, \mathrm{d}r,$$

averaged over the whole ring; a periodicity condition on Ψ was imposed at $\phi = 0$, $2\pi/n_0$.

This procedure differs from that of Sommeria *et al.* in that we introduced step (ii) based on the axial symmetry of the flow studied. The effect of this step is to remove

random variations in different vortices and to drastically increase streak density, providing much more precise and detailed results. In fact, we had about 2000–3000 tracks per single ('composite') vortex yielding spatial resolution of about 2–3 mm.

Almost every step adds a certain amount of error in the data. Errors in locating streaks, uncertainty of interpolation on 'blank' domains (where there are no or few visualizer particles) and amplification of errors in numerical differentiation are possibly the most significant. However, step (v) improves the net result.

To show this, note that the interpolated velocity field has non-zero divergence due to errors. On the other hand, the resulting stream function describes non-divergent 2D flow. How is it related to the experimental velocity field $\boldsymbol{v}_e$? Let us seek a non-divergent field $\boldsymbol{v}_t$, being the best fit for $\boldsymbol{v}_e$ in the sense of least squares, $\iint |\boldsymbol{v}_t - \boldsymbol{v}_e|^2 \,dx\,dy \to \min$. On substituting $\boldsymbol{v}_t = \nabla \times (\Psi \boldsymbol{e}_z)$ into the above integral and varying Ψ we obtain equation (2). So (2) yields the best non-divergent fit to the interpolated experimental velocity field, and step (v) does reduce measurement and interpolation errors (at least those which bring about divergence). Note that errors due to numerical differentiation are also reduced, as the stream function is obtained by double integration of the vorticity. An example of flow patterns and corresponding streamlines ($\Psi = \text{const}$) is provided by figure 2 (the photos in figure 2 are but illustrative examples; they provide no distinct streaks). One can see that the aluminium powder is inhomogeneously distributed on the fluid surface. For instance, for the sine-type profile flow (figure 2*a*) there are no valid tracks in the small vortices near the inner channel wall. The calculated stream function, nevertheless, reveals these vortices.

For Kolmogorov flow we used only a central zone of 6.4×17.6 cm (6.4 cm is the longitudinal period of the vortex pattern). Step (ii) (superposition of periods) was left out in this case because of lack of translational symmetry. Only in the central zone is the flow free of distortions due to endwalls of the cuvette. The total number of tracks in this zone was about 4000–5000.

5. Mean velocity, mean vorticity and Reynolds stresses

Transverse profiles of mean azimuthal velocity $\langle v_\phi \rangle$ and Reynolds stresses $\langle v_\alpha v_\beta \rangle$ (α, β stand for r or ϕ, angular brackets denote an average over ϕ) are presented in figure 3. This figure demonstrates that the $\langle v_\phi v_r \rangle$ component which characterizes the mean azimuthal transfer of radial momentum, is concentrated about inflexion points of the mean velocity profile. Note that the difference in velocity profiles between sine-type and tanh-type flows, though comparatively small, causes an essential difference in the profiles of $\langle v_\phi v_\phi \rangle$ and $\langle v_\phi v_r \rangle$. For the tanh-type flow the concentration is more pronounced. The $\langle v_r v_r \rangle$ component, which can be treated as the squared amplitude of the vortex disturbance, is spread widely around the inflexion point.

In accordance with weakly nonlinear theory and with previous experimental results of Krymov (1989), the Reynolds stresses depend linearly on supercriticality $s = \mathbb{R}_\lambda / \mathbb{R}_\lambda^* - 1$ (see figure 4). This corresponds to a subcritical instability and is consistent with the Hopf bifurcation theory, according to which the disturbance amplitude is proportional to the square root of the controlling external parameter. The slope of the above-mentioned linear dependence was shown in Manin (1989) to be highly sensitive to the velocity profile of the primary flow. The present experimental data appear to be consistent with this result. Normalized slopes $\eta_{\alpha\beta} = (\mathrm{d}/\mathrm{d}s) \langle v_\alpha v_\beta \rangle / U^{*2}$ are presented in table 1, where U^* is the critical velocity of the primary flow. They vary significantly for different flows, but ratios of these values

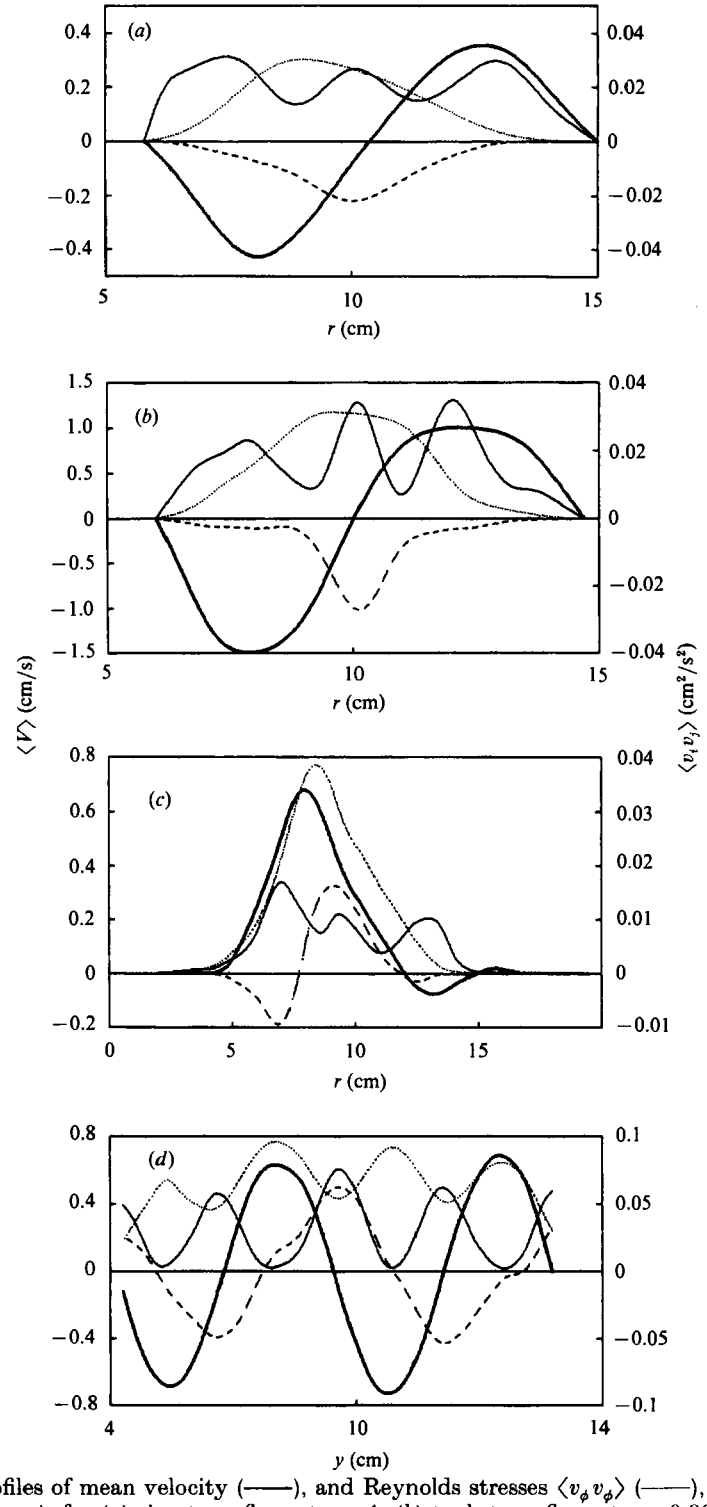

FIGURE 3. Profiles of mean velocity (——), and Reynolds stresses $\langle v_\phi v_\phi \rangle$ (——), $\langle v_r v_r \rangle$ (· · · · · ·) and $\langle v_r v_\phi \rangle$ (– – – –), for (*a*) sine-type flow at $s = 1$, (*b*) tanh-type flow at $s = 0.86$, (*c*) jet flow at $s = 1.85$, (*d*), and Kolmogorov flow at $s = 0.53$

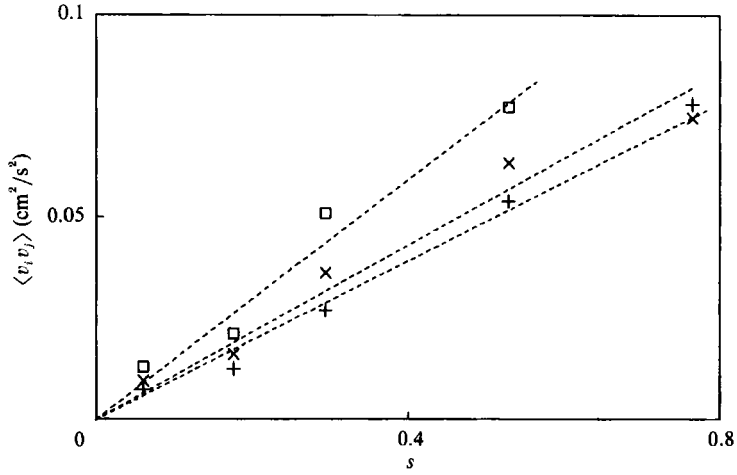

FIGURE 4. Dependence of amplitude of Reynolds stresses $\langle v_x v_x \rangle$ (□), $\langle v_y v_y \rangle$ (+), and $\langle v_x v_y \rangle$ (×), on supercriticality s for Kolmogorov flow.

Flow	Sine	Tanh	Jet	Kolmogorov
h (cm)	1.0	0.5	0.7	0.4
U'	0.22	0.73	0.315	0.22
η_{rr}	0.23	0.067	0.117	0.264
$\eta_{r\phi}$	−0.153	−0.0675	−0.0722	−0.252
$\eta_{\phi\phi}$	0.17	0.07	0.013	0.37
E_{ψ_1}	97%	93%	98%	98%
λ	0.038±0.004	0.14±0.02	0.043±0.002	0.234±0.02
κ	1.7±0.2	1.6±0.2	0.96±0.04	1.7±0.15

TABLE 1. Measured parameters for the various flow types

(such as $\eta_{rr}/\eta_{r\phi}$) vary only weakly. So $\eta_{\alpha\beta}$ can be taken as a measure of the squared amplitude of the disturbance.

The disturbance amplitude manifests itself not only in vortex intensity, but also in the size and shape of vortices. At larger Reynolds numbers the vortices are more rounded and more tilted. In Krymov (1989) it was shown that the slopes of the dependence of width and tilt of vortices can in the same sense serve as a measure of amplitude. Note also that there is no correlation between these values and the depth h of the fluid layer.

Profiles of mean azimuthal velocity and mean vorticity are presented in figure 5 for the tanh-type flow at various s. The dashed line was obtained by direct measurement of tracks rather than from the stream function at $s = 0$. It is close to the calculated velocity profile at small supercriticality $s = 0.14$ (solid curve 1). This figure illustrates the spreading of the shear zone with increasing s under the reverse action of vortices on the primary flow. This spreading is more pronounced in the vorticity profiles (figure 5b). The shear zone (the domain of high vorticity) widens at the expense of nearly constant velocity domains, so that the vorticity amplitude increases with Reynolds number more slowly than the velocity amplitude.

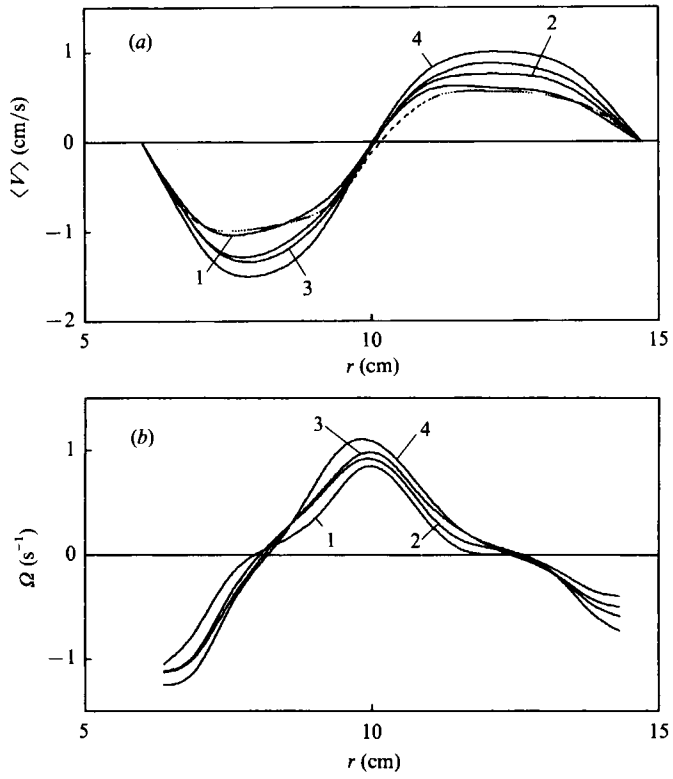

FIGURE 5. (*a*) Mean velocity and (*b*) vorticity profiles for the tanh-type flow at $s = 0.14$ (curves 1); 0.43 (2); 0.57 (3); 0.86 (4). Dashed line on (*a*) show the mean velocity profile at the critical Reynolds number obtained by direct measurement of tracks rather than the stream-function calculation.

6. The harmonic analysis of disturbances

Stream functions obtained from streak photographs are detailed enough to provide more delicate characteristics of the flow. Recall that weakly nonlinear theory is not restricted to treatment of a purely harmonic disturbance, but also accounts for its interaction with the second longitudinal harmonic and with weak distortion of the primary flow (both resulting from interaction of the principal wave with itself). Write the stream function of the secondary flow in the form

$$\Psi = \Psi_0(y) + \psi(x, y),$$

$$\psi(x, y) = \mathrm{Re} \sum \psi_k(y) \exp(ik\alpha_0 x)$$

(for simplicity this is written in Cartesian coordinates as if the flow were rectilinear). Then ψ_1 is the principal harmonic and ψ_2 is the second harmonic. Hodographs of ψ_1 and ψ_2 for different flows are presented in figure 6 (by a hodograph of $\psi(y) \subset \mathbb{C}$ we mean a plot of the imaginary part *vs.* the real part of ψ as an implicit function of y). Dashed lines correspond to experimental data, while solid lines were obtained by numerical integration of Rayleigh-type equations arising in the course of the realization of the Stuart–Watson weakly nonlinear scheme (Stuart 1960; Watson 1960). Note that theoretical curves correspond to perfect velocity profiles $U = \sin y$ and $U = \tanh y$, rather than to experimental profiles. This is because the theoretical procedure requires information on higher derivatives (up to the third) of $U(y)$, which is not available from the experiment. We are interested here only in the

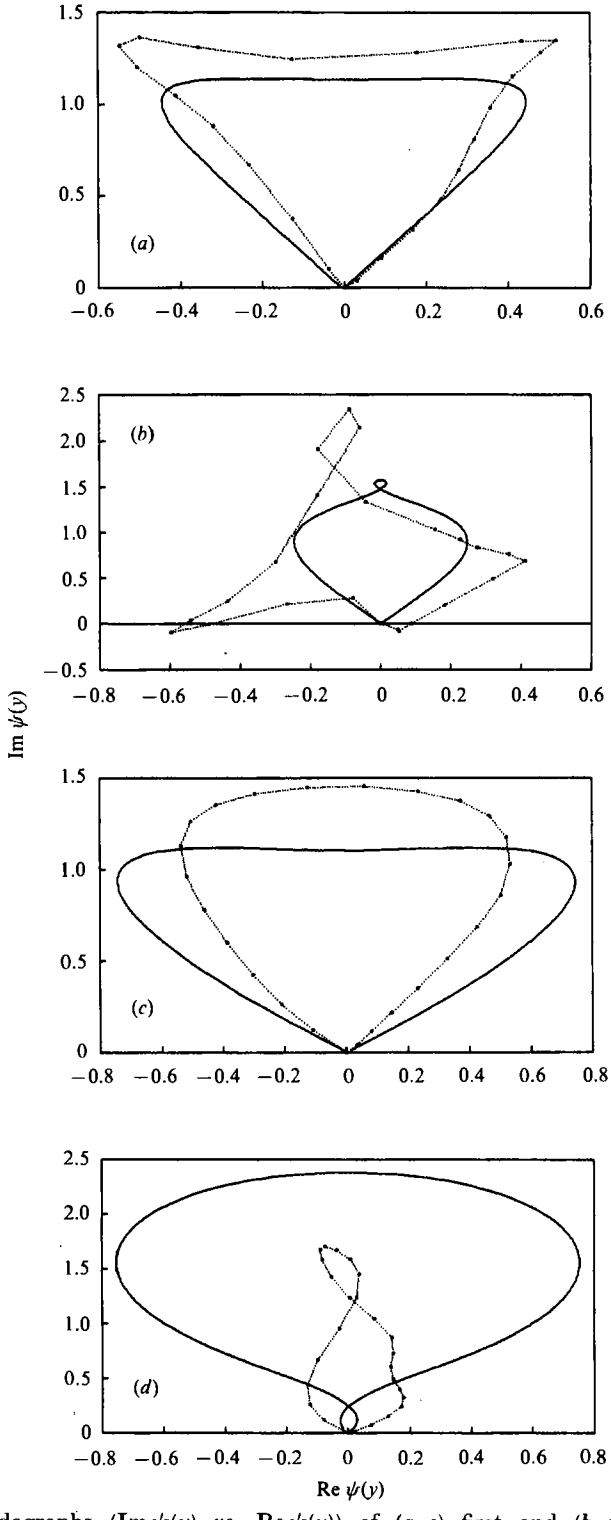

FIGURE 6. Hodographs ($\mathrm{Im}\,\psi(y)$ *vs.* $\mathrm{Re}\,\psi(y)$) of (a, c) first and (b, d) second harmonic of disturbances for (a, b) tanh-flow and (c, d) sine-type flow. Dashed lines correspond to experimental data, solid lines to weakly nonlinear theory (Manin 1989).

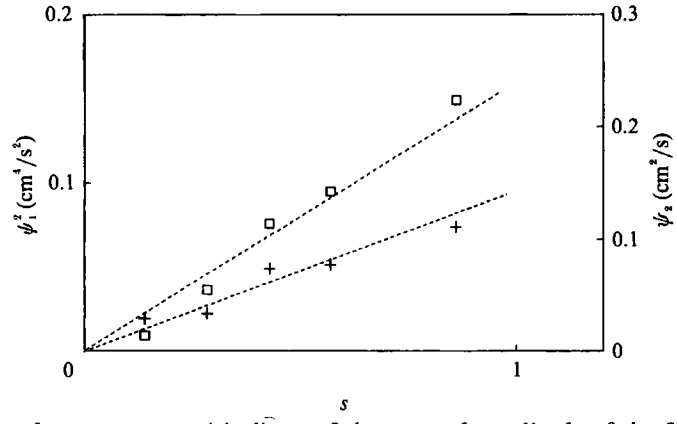

FIGURE 7. Dependence on supercriticality s of the squared amplitude of the first harmonic of disturbances (□) and the amplitude of the second (+), for tanh-type flow.

shape of these hodographs, so every curve is normalized by the condition r.m.s. $(\mathrm{Im}^2+\mathrm{Re}^2)=1$.

Figure 6 illustrates that the theoretical and experimental hodographs are 'topologically' similar. Note also that the difference in velocity profiles affects the second harmonic more strongly. The shape of the hodograph loop is in fact quite meaningful. Let us express the Reynolds stress $\langle v_x v_y \rangle$ as a sum of terms, each due to a specific harmonic, ψ_k. It can be easily shown that the sign of every term is determined by the sign of $(\mathrm{d}/\mathrm{d}y)(\arg\psi_k(y))$. But the sign of the Reynolds stress in turn determines the sign of energy transfer – from mean flow to vortices or the reverse, because $\nu_e = -\langle v_r v_\phi \rangle / U'$ determines the 'eddy viscosity'. This quantity was shown by Dovzhenko & Krymov (1983) to be almost constant across the flow. Now we can analyse contributions of harmonics to the energy exchange between the mean flow and vortices. Figure 6 demonstrates that while the first harmonic only takes energy from the mean flow, the second harmonic partially returns it (reverse loops in hodographs).

According to weakly nonlinear theory, the amplitude of the second harmonic should be proportional to the supercriticality s, rather than to $s^{\frac{1}{2}}$ (figure 7). We were able to check this only with the tanh-type flow, since in the other cases the second harmonic was extremely small, so that almost all the energy of the disturbance was contained in the principal harmonic. The average fraction of the disturbance 'energy' (integral of ψ^2) which is due to the principal harmonic is shown in table 1 as E_{ψ_1}. The smallness of higher harmonics indicates that flow really is weakly nonlinear.

7. Reconstruction of pressure fields

The pressure field is of interest both in itself and for subsequent data processing. Apply the divergence operator to the stationary form of the governing Q2D equation (1),

$$(\boldsymbol{v}\cdot\nabla)\,\boldsymbol{v} = -\nabla p - \lambda \boldsymbol{v} + \boldsymbol{f}.$$

Taking into account the continuity equation $\nabla\cdot\boldsymbol{v}=0$ and assuming the force non-divergent, $\nabla\cdot\boldsymbol{f}=0$, we obtain the well-known Poisson equation for pressure,

$$\nabla^2 p = 2[u, v], \tag{3}$$

where square brackets denote the Jacobian, $[F, G] = F_x G_y - F_y G_x$. The Jacobian $[u, v]$ may be treated (up to a constant factor) as the Gaussian curvature of the stream function considered as a surface $\Psi = \Psi(x, y)$ in the (x, y, Ψ)-space. Negative curvature corresponds to 'hyperbolic' streamlines, positive curvature to 'elliptic' streamlines. This may be the reason why isobars reveal vortices better than streamlines (see figure 2).

It is essential that only first-order spatial derivatives enter the right-hand side of (3), because additional numerical differentiation would make results much less reliable. Equation (3) was integrated in cylindrical coordinates with boundary conditions of the form $\partial_r p = v_\phi^2/r = 0$ at $r = r_1, r_0$, which follows from the radial component of the momentum equation (since in the real flow we have $v_\phi = 0$ at lateral boundaries). The periodicity condition in ϕ was also imposed on p.

The most prominent feature of the pressure field is the depression at the centre of a vortex. For jet flow, alternating minima and maxima of p reflect the wavy pattern of streamlines. For axially symmetric flows there is a systematic rise of pressure from the inner to the outer boundary, due to curvature of the primary flow.

8. Testing the Q2D approximation

The applicability of the governing Q2D equation (1) is confirmed by its ability to predict stability characteristics of laboratory flows, demonstrated by Krymov (1989) and Krymov & Manin (1989). Nevertheless it is especially interesting to test it directly by immediate substitution of the experimental velocity field into (1). Let us rewrite (1) in terms of velocity components (we again simplify formulae by assuming the flow rectilinear; actual calculations for axially symmetric flows were made in cylindrical coordinates):

$$u\frac{\partial u}{\partial x} + v\frac{\partial u}{\partial y} = -\frac{\partial p}{\partial x} - \lambda u + f, \tag{4}$$

$$u\frac{\partial v}{\partial x} + v\frac{\partial v}{\partial y} = -\frac{\partial p}{\partial y} - \lambda v, \tag{5}$$

$$u = \frac{\partial \Psi}{\partial y}, \quad v = -\frac{\partial \Psi}{\partial x}.$$

Equation (5) can be used to determine λ by taking the pressure term over to the left-hand side and calculating the regression coefficient between the left-hand side and v, where u, v and p are experimental fields. Owing to measurement errors and additional numerical differentiation, the regression analysis yields rather low correlation coefficients. But because of the large number of grid points, the overall average λ value can be considered realistic. The λ-independence of the Reynolds number for a given flow would be evidence of its correctness.

In fact the dispersion of λ for every flow type at various s turned out to be about 10% or less (see table 1). Moreover, for three flow types (except the jet) λ is given by

$$\lambda = 2\kappa\nu/h^2, \tag{6}$$

with $\kappa = 1.7 \pm 0.2$. This is strong evidence in favour of the Q2D model.

The value of the phenomenological parameter κ depends critically on the actual vertical profile of velocity (in particular, for a Poiseuille vertical profile κ would be equal to 1; see Gledzer *et al.* 1981). For jet flow, as distinct from other flows, the electric current density decreases sharply from the bottom to the free surface. The resulting difference in vertical velocity profile leads to a different κ value.

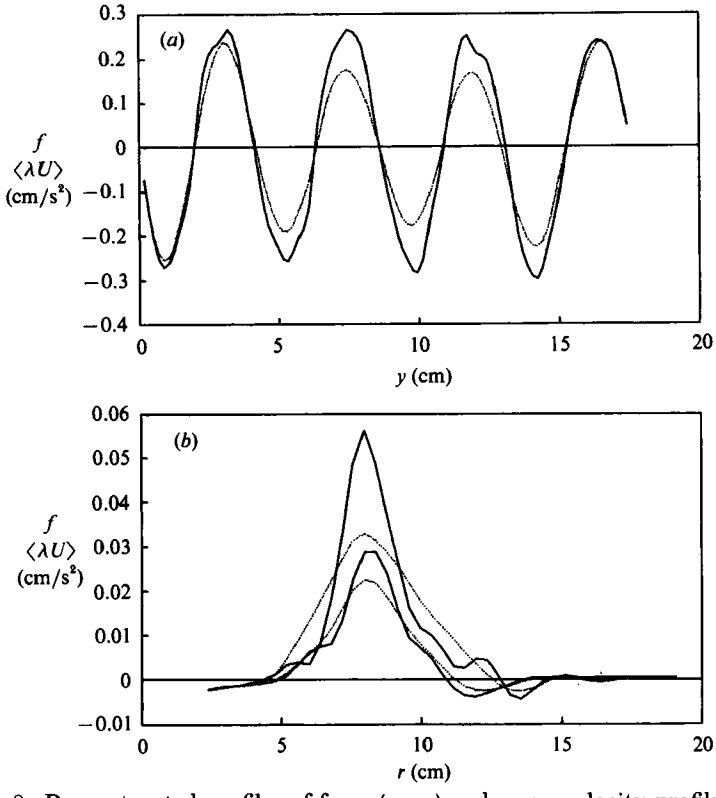

FIGURE 8. Reconstructed profiles of force (——) and mean velocity profiles (multiplied by λ) (· · · · · ·), for (*a*) Kolmogorov flow at $s = 0.76$ and (*b*) jet flow at $s = 0.71$ and 2.57.

Now that λ is known we can substitute experimental fields into (4) to reconstruct the force. Profiles of force and of mean longitudinal velocity (multiplied by λ) are presented in figure 8. Since the flow is stationary, the difference between f and λU shows the contribution of nonlinear terms in (4), that is, the reverse action of vortices on the primary flow. (We show the results for Kolmogorov and jet flows where this contribution affects not only the amplitude of the velocity profile, but also its shape.)

Figure 8(*a*) demonstrates that for Kolmogorov flow the reconstructed force is of constant amplitude across the cuvette (as it should be), while the mean velocity is lower in the middle where vortices are stronger. For the jet (figure 8*b*) the instability causes the mean flow to spread, while the width of the force profile remains constant. This is also shown in figure 9 (to determine the width D of a profile we approximated it by $U = U_0 \exp(-(r-R_0)^2/D^2)$.

Figure 10 shows the dependence of the amplitudes of f and λU on s for these two flows. One can see that the amplitude of the force is proportional to the Reynolds number (recall that it is proportional to the net electric current). At the same time the mean flow velocity dependence changes at the critical Reynolds number ($s = 0$) because developing vortices take the energy from the primary flow. In table 1 the normalized slope of this dependence in supercritical regime is presented, $U' = (\mathrm{d}U/\mathrm{d}s)/U^*$.

The simplest possible three-mode Galerkin model of Kolmogorov flow (Dolzhanskii *et al.* 1990) predicts completely constant mean flow velocity at $s > 0$. The weak growth of mean velocity observed in experiments can be related to the presence of

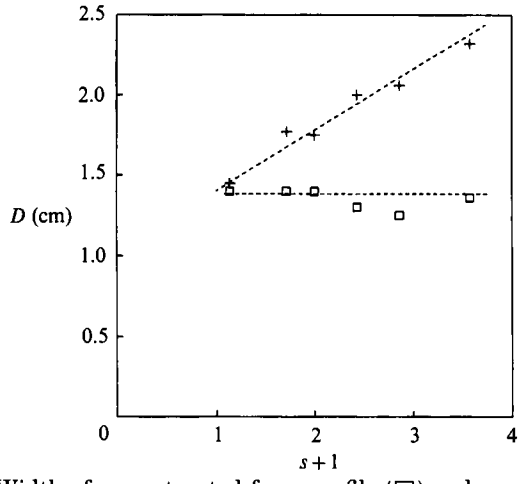

FIGURE 9. Width of reconstructed force profile (□) and mean velocity profile (+) *vs.* supercriticality for jet flow.

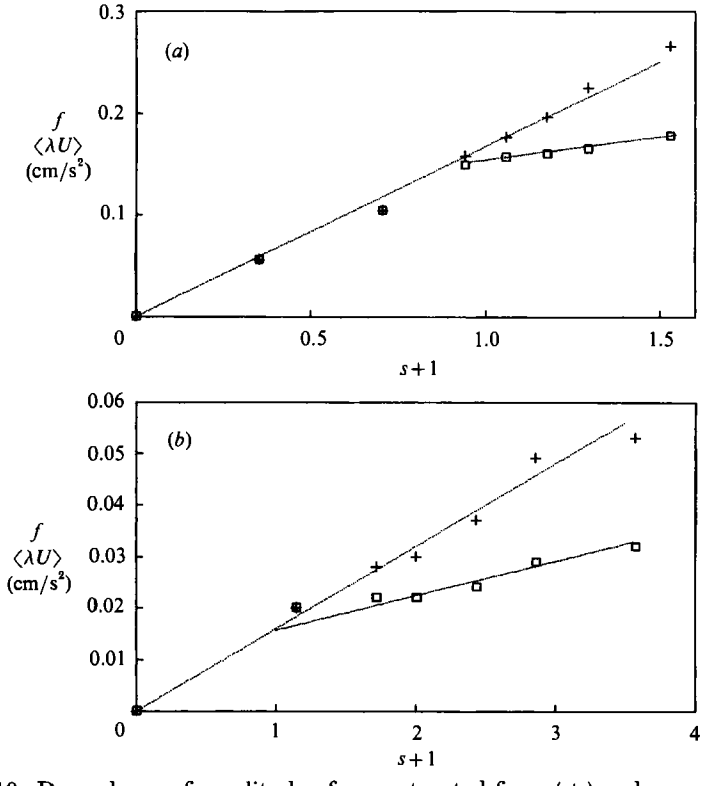

FIGURE 10. Dependence of amplitude of reconstructed force (+) and mean velocity (multiplied by λ) (□) on supercriticality for (*a*) Kolmogorov, and (*b*), jet flows.

second and higher harmonics, since they can partially return energy obtained from the principal harmonic back to the mean flow (see above). This is consistent with data in table 1: the greater the relative amplitude of the second harmonic, the greater the slope of mean velocity dependence on s and the smaller the total energy

of disturbances ($\eta_{\alpha\beta}$). In addition, it can be shown that the four-mode Galerkin model of Kolmogorov flow which takes into account the second harmonic of a disturbance yields qualitatively the same behaviour as in the experiment.

9. Conclusions

Two principal results of the present work deserve being stated here as conclusions.

(i) There is direct experimental verification of the quasi-two-dimensional approximation (1) for thin-layer viscous fluid motions. The applicability of the Q2D approximation follows from the non-dependence of the external friction coefficient λ (calculated under the assumption of quasi two-dimensionality) on the Reynolds number, and from that the λ value is given by (6) with a unique κ for different velocity profiles and layer thicknesses.

(ii) The possibility of reconstructing the force driving a Q2D shear motion has been demonstrated. Correct behaviour was obtained for both profile of the force (independent of Reynolds number in our set-up) and its amplitude (proportional to the net electric current).

The theory of Q2D flows can be applied to barotropic atmospheric flows (see the review by Dolzhanskii *et al.* 1990). The problem of reconstruction of non-adiabatic factors (such as heat and potential vorticity sinks/sources) is urgent in dynamical meteorology. The method proposed here cannot be directly applied to the atmosphere, for this would require resolution of the vertical structure. However, given the data on horizontal fields at different altitude levels, the procedure could be generalized for reconstruction of the right-hand side of the potential vorticity transformation equation.

REFERENCES

Busse, F. H. 1968 Shear flow instabilities in rotating fluid. *J. Fluid Mech.* **33**, 577–589.

Chomaz, J. M., Rabaud, M., Basdevant, C. & Couder, Y. 1988 Experimental and numerical investigation of a forced circular shear layer. *J. Fluid Mech.* **187**, 115–140.

Dolzhanskii, F. V. 1987 On the effect of external friction on the stability of plane parallel shear flows. *Izv. Acad. Sci. USSR. Atmos. Ocean. Phys.* **23**, 348–356.

Dolzhanskii, F. V., Krymov, V. A. & Manin, D. Yu. 1990 Stability and vortex structures of quasi two-dimensional shear flows. *Usp. Fiz. Nauk.* **160** (7), 1–47 (transl. in *Sov. Phys. Usp.* **33** (7), 495–520).

Dolzhanskii, F. V., Krymov, V. A. & Manin, D. Yu. 1991 Quasi two-dimensional coherent structures. In *Non-linear Dynamics of Structures (Perm-Moscow, 11–20 June 1990)* (ed. R. Z. Sagdeev, U. Frisch, A. K. M. F. Hussein, S. S. Moiseev & N. Erokhin), pp. 1–20. World Scientific.

Dolzhanskii, F. V. & Manin, D. Yu. 1990 Free shear layers and laboratory simulation of atmospheric circulation. *Izv. Acad. Sci. USSR. Atmos. Ocean. Phys.* **26**, 1282–1288.

Dovzhenko, V. A. & Krymov, V. A. 1983 Momentum transfer by vortices in an unstable plane axially symmetric shear flow. *Izv. Acad. Sci. USSR. Atmos. Ocean. Phys.* **19**, 534–539.

Dovzhenko, V. A., Novikov, Yu. V. & Oboukhov, A. M. 1979 Laboratory simulation of vortex generation in an axially symmetric azimuthal field by MHD method. *Izv. Acad. Sci. USSR. Atmos. Ocean. Phys.* **15**, 1199–1202.

Gledzer, E. B., Dolzhanskii, F. V. & Oboukhov, A. M. 1981 *Hydrodynamic-Type Systems and Their Applications*. Moscow: Nauka.

Krymov, V. A. 1989 Stability and supercritical regimes of quasi two-dimensional shear flows with external friction (experiment). *Izv. Acad. Nauk USSR. Mekh. Zhidk. Gaza* (transl. in *Fluid Dyn.*) **2**, 12–18.

Krymov, V. A. & Manin, D. Yu. 1989 Linear and non-linear stability of quasi two-dimensional jet flows with external friction. *Izv. Acad. Sci. USSR. Atmos. Ocean. Phys.* **25**, 234–242.

MANIN, D. YU. 1989 Stability and supercritical regimes of quasi two-dimensional shear flows with external friction (theory). *Izv. Acad. Sci. USSR. Mekh. Zhidk. Gaza* (transl. in *Fluid Dyn.*) **2**, 19–27.

NIINO, H. 1982 A weekly non-linear theory of barotropic instability. *J. Met. Soc. Japan* II **60**, 1001–1023.

NIINO, H. & MISAWA, N. 1984 An experimental and theoretical study of barotropic instability. *J. Atmos. Sci.* **41**, 1992–2011.

RABAUD, M. & COUDER, Y. 1983 A shear-flow instability on a circular geometry. *J. Fluid Mech.* **136**, 291–319.

SOMMERIA, J., MEYERS, S. & SWINNEY, H. 1989 Experiment on vortices and Rossby waves in eastward and westward jets. In *Nonlinear Topics in Ocean Physics: Intl School of Phys. Enrico Fermi. Varenna, 26 July – 5 Aug. 1988* (ed. A. Osborne). North-Holland.

STUART, J. T. 1960 On the non-linear mechanics of wave disturbances in stable and unstable parallel flows. Part 1. The basic behaviour in plane Poisuille flow. *J. Fluid Mech.* **9**, 353–370.

WATSON, J. 1960 On the non-linear mechanics of wave disturbances in stable and unstable parallel flows. Part 2. The development of a solution for plane Poiseuille flow and for plane Couette flow. *J. Fluid Mech.* **9**, 371–389.